

ON THE BEHAVIOR OF CONED-FACE AND MISALIGNED SPIRAL GROOVE GAS FACE SEALS

Marco Tulio C. Faria

Department of Mechanical Engineering
Federal University of Minas Gerais
Av. Antonio Carlos, 6627
31270-901 - Belo Horizonte, MG - Brazil
mtfaria@demec.ufmg.br

Abstract. *This work deals with a finite element analysis of gas-lubricated spiral groove face seals operating under stringent conditions. Seal face misalignment and coning effects are accounted for in the numerical model specially devised for the computation of some steady-state and dynamic performance characteristics of gas face seal operating at high speeds. A high-order Galerkin scheme is implemented to solve the zeroth- and first-order lubrication equations generated by the perturbation procedure carried out on the classical non-linear Reynolds equation for compressible fluids. The gas seal opening force, leakage flow and dynamic force coefficients are predicted for misaligned and coned-face spiral groove seals for several operating conditions. Numerical results depict the influence of angular misalignment and face coning on the behavior of gas lubricated spirally grooved face seals.*

Keywords. *Gas Seals, Face Seals, Spiral Grooves, Angular Misalignment, Face Coning.*

1. Introduction

Gas face seals are finding increase use in industrial turbomachinery that requires efficient sealing systems and high productivity. Most of the very efficient sealing systems for industrial turbomachinery are based on grooved face seals, whose grooves can have different geometries, such as spiral grooves, T-grooves, U-grooves and others (Burgmann, 1997).

Demands for more efficiency and higher productivity have led the face seals to be operated under very stringent conditions. Varying high pressure ratios combined with almost inevitable geometric imperfections can induce instantaneous angular motions on the face seal plates, which can drastically change the seal performance (Sharoni and Etsion, 1981). At very high operating speeds, large pressure ratios and thermal distortions can make the face seal susceptible to angular motions and coning effects (Pan and Sternlicht, 1967). Some studies developed on liquid-lubricated face seals have verified that the seal face angular misalignment and coning affect the seal performance and efficiency, jeopardizing its capability of working properly (Metcalf, 1981, and Wileman and Green, 1991). On the other hand, even though the importance of the seal dynamics on the analysis of gas lubricated sealing systems has already been demonstrated (Tournerie et al, 1994), the technical literature lacks technical data about steady-state and dynamic performance characteristics of the misaligned and the coned-face gas lubricated seals operating at high speeds.

This work deals with a finite element analysis of spiral groove gas face seals (SGGFSs) operating at high speeds, which accounts for the face angular misalignment and coning effects. A finite element procedure, which is based on a high-order Galerkin scheme (Faria, 2001), is implemented to solve the zeroth- and first-order lubrication equations in grooved gas seals. The numerical model includes both the angular misalignment modeling (Faria, 2002) and the face coning motion formulation. Some steady-state and dynamic performance characteristics of misaligned and coned-face spiral groove gas seals, such as opening force, flow leakage and force coefficients, are evaluated at high operating speeds. The numerical results depict the influence of the angular misalignment and the face coning on the behavior of spiral groove gas face seals operating under very demanding operating conditions.

2. Parameters and Governing Equation for a SGGFS

The geometry and parameters that describe a spiral groove gas face seal (SGGFS) are depicted in Fig. (1). The seal configuration is described following the same procedure as that used by Faria (2002). The seal geometry includes the ridge clearance c , the groove depth c_g , the ridge width w_r , the groove width w_g , the number of grooves N_g , the groove angle β , the seal inner radius r_i , the seal outer radius r_o , the seal grooved portion inner radius r_{gi} and the seal grooved portion outer radius r_{go} . The groove depth ratio $\delta = c_g/c$, the groove width ratio $\alpha_g = w_g/(w_r + w_g)$ and the seal dam extent $l = (r_{gi} - r_i)/(r_o - r_i)$ are dimensionless geometric parameters widely used in the description of the seal geometry. The seal configuration is described in relation to a coordinate system attached to the grooved seal face. The (r, θ, z) coordinate system is attached to the rotating grooves at speed Ω . The (r, Φ, z) coordinate system is attached to the stationary face. The relation between the two coordinate systems is given by $\Phi = \theta + \Omega t$. The equation governing the logarithmic spiral contour of the grooves is $r = r_{gi} e^{\theta \tan(\beta)}$ (Muijderman, 1966). Grooves are etched either on the rotating surface or on the stationary surface of the seal. The relative motion between the grooved and smooth surfaces causes a pumping action in the fluid. Pumping-in (inwardly pumping) and pumping-out (outwardly pumping) seal

designs usually find applications in industrial rotating machinery (Muijderman, 1966). Sealing pressure dams are generally employed in SGGFS configurations either to minimize leakage or increase axial stiffness. Inner and outer pressure dams are introduced into the grooved surface to enhance the seal performance.

The laminar flow of an isothermal, isoviscous ideal gas within the film lands of a spirally grooved face seal (Faria, 2001) is described by

$$\frac{1}{r} \frac{\partial}{\partial \theta} \left(\frac{ph^3}{12\mu} \frac{1}{r} \frac{\partial p}{\partial \theta} \right) + \frac{1}{r} \frac{\partial}{\partial r} \left(\frac{ph^3}{12\mu} r \frac{\partial p}{\partial r} \right) = \frac{B\Omega}{2r} \frac{\partial}{\partial \theta} (rph) + \frac{\partial (ph)}{\partial t} \quad (1)$$

Here, p represents the hydrodynamic pressure, h is the fluid film thickness, and μ is the fluid viscosity. B is a seal parameter that describes the groove rotation direction. The values of B for the different seal configurations are given in Faria (2001).

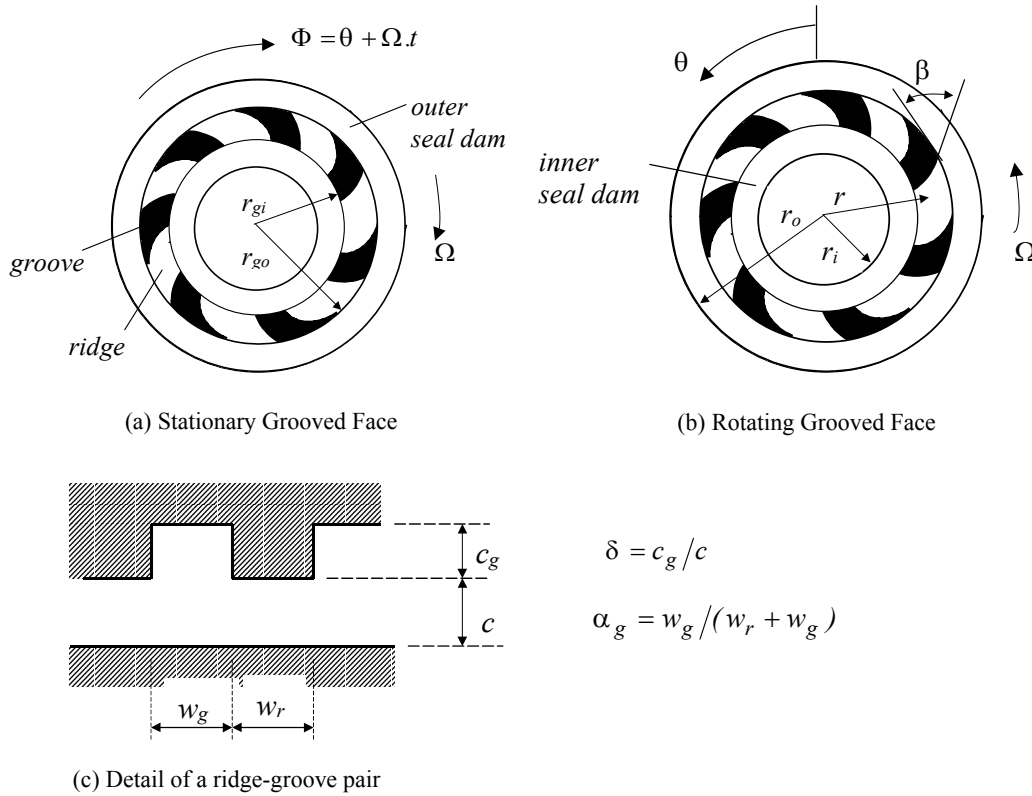


Figure 1. Description of a SGGFS with rotating and stationary grooved face.

The seal is subjected to pressures p_{in} and p_{out} at its inner and outer radii r_i and r_o , respectively. Typically $p_{out} > p_{in}$. In a seal, the inner and outer radii sections are open allowing radial flow inward and outward. The pressure distribution is periodic over the seal/bearing circumferential length. The fluid film thickness is described accounting for both the static misalignments of the seal surface (Jang and Kim, 1999) and the face coning. Figure (2) shows a schematic view of a coned face mechanical seal. The seal moving surface has basically three degrees of freedom, schematically shown in Fig. (3).

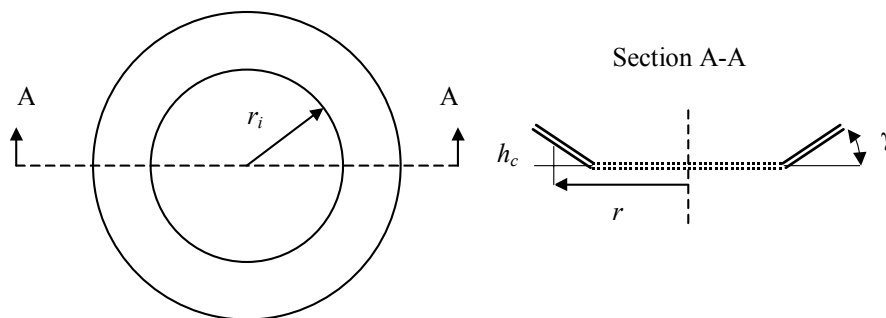


Figure 2. Schematic view of a coned face mechanical seal.

The film thickness h_o at an equilibrium position can be written as

$$h_o(r, \theta) = c + r\phi_{y_o} \cos \theta - r\phi_{x_o} \sin \theta + h_c(r), \quad \text{in the ridge region} \quad (2)$$

$$h_o(r, \theta) = c + c_g + r\phi_{y_o} \cos \theta - r\phi_{x_o} \sin \theta + h_c(r), \quad \text{in the groove region.} \quad (3)$$

ϕ_{x_o} and ϕ_{y_o} describe the angular position of the moving surface at equilibrium, i.e. are small angular displacements representing the face misalignment about axes X and Y , respectively. The coning effects are given by $h_c(r) = (r - r_i) \tan \gamma$, where γ represents the coning angle of the seal surface (see Fig. (2)). The seal mating faces are manufactured with compatible materials of different moduli of elasticity and coefficients of thermal expansion (Burgmann, 1997). The face with lower modulus of elasticity and coefficient of thermal expansion is more likely subjected to face coning.

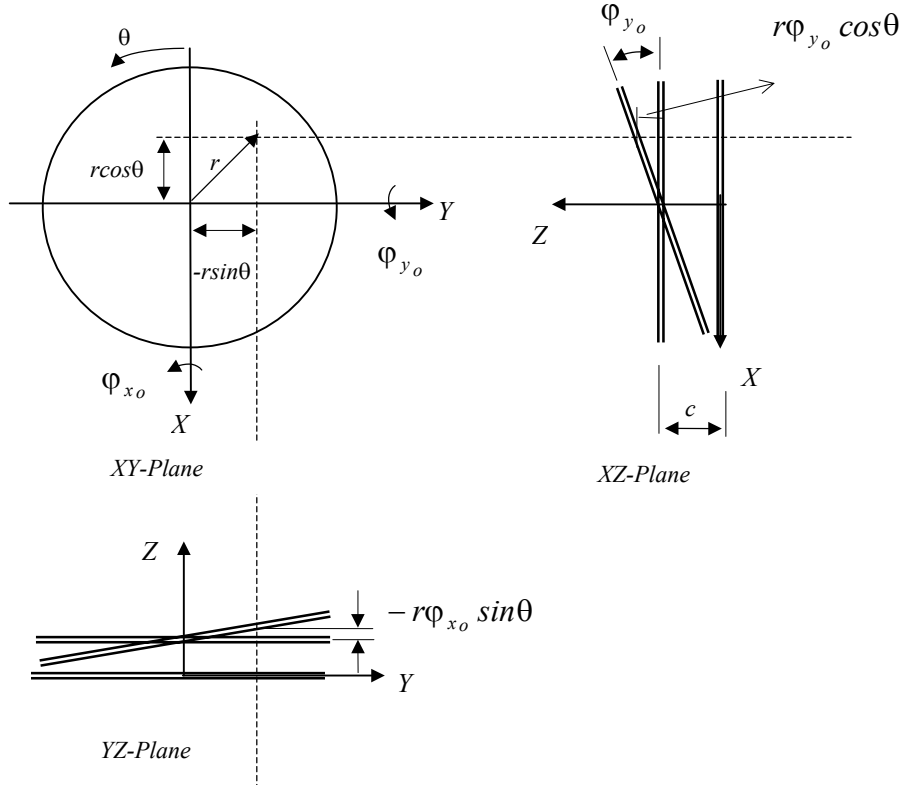


Figure 3. Equilibrium position of a misaligned moving surface.

3. Lubrication Equations

A linearized perturbation procedure (Lund, 1987) is performed on the Reynolds equation (Eq. (1)) to render the zeroth- and first-order lubrication equations. Small dynamic perturbations ΔZ , $\Delta \phi_x$, and $\Delta \phi_y$ at excitation frequency ω about an equilibrium position of the moving rotating face cause perturbations in the film thickness and pressure distributions. The perturbed film thickness $h(r, \theta, t)$ is given by

$$h(r, \theta, t) = h_o(r, \theta) + r \cos \theta \cdot \Delta \phi_y e^{i\omega t} - r \sin \theta \cdot \Delta \phi_x e^{i\omega t} + \Delta Z \cdot e^{i\omega t} \quad (4)$$

where $i = \sqrt{-1}$. The perturbed pressure field is expressed as

$$p(r, \theta, t) = p_o(r, \theta) + p_z(r, \theta) \Delta Z e^{i\omega t} + p_{\phi_x}(r, \theta) \Delta \phi_x e^{i\omega t} + p_{\phi_y}(r, \theta) \Delta \phi_y e^{i\omega t} \quad (5)$$

where p_o represents the zeroth-order pressure field, and p_z , p_{ϕ_x} , and p_{ϕ_y} are the first-order pressure distributions caused by the small perturbations. Expressions for the linearized zeroth- and first-order lubrication equations are obtained by substituting Eq. (4) and Eq. (5) into Eq. (1). The zeroth-order lubrication equation has the following form.

$$\frac{1}{r} \frac{\partial}{\partial \theta} \left(\frac{p_o h_o^3}{12\mu} \frac{1}{r} \frac{\partial p_o}{\partial \theta} - \frac{B\Omega r}{2} p_o h_o \right) + \frac{1}{r} \frac{\partial}{\partial r} \left(\frac{p_o h_o^3}{12\mu} r \frac{\partial p_o}{\partial r} \right) = 0 \quad (6)$$

The first-order equation for axial displacement Z is expressed as

$$\begin{aligned} & \frac{1}{r} \frac{\partial}{\partial \theta} \left(\frac{3h_o^2}{12\mu r} p_o \frac{\partial p_o}{\partial \theta} + \frac{h_o^3}{12\mu r} \frac{\partial(p_o p_z)}{\partial \theta} - \frac{B\Omega r}{2} (p_z h_o + p_o) \right) + \\ & \frac{1}{r} \frac{\partial}{\partial r} \left[r \left(\frac{3h_o^2}{12\mu} p_o \frac{\partial p_o}{\partial r} + \frac{h_o^3}{12\mu} \frac{\partial(p_o p_z)}{\partial r} \right) \right] = i\omega (p_z h_o + p_o) \end{aligned} \quad (7)$$

The first-order equations for the dynamic angular displacements φ_x and φ_y around the X and Y axes are given by

$$\begin{aligned} & \frac{1}{r} \frac{\partial}{\partial \theta} \left(\frac{-3h_o^2 r \sin\theta}{12\mu r} p_o \frac{\partial p_o}{\partial \theta} + \frac{h_o^3}{12\mu r} \frac{\partial(p_o p_{\varphi_x})}{\partial \theta} - \frac{B\Omega r}{2} (p_{\varphi_x} h_o - p_o r \sin\theta) \right) + \\ & \frac{1}{r} \frac{\partial}{\partial r} \left[r \left(\frac{-3h_o^2 r \sin\theta}{12\mu} p_o \frac{\partial p_o}{\partial r} + \frac{h_o^3}{12\mu} \frac{\partial(p_o p_{\varphi_x})}{\partial r} \right) \right] = i\omega (p_{\varphi_x} h_o - p_o r \sin\theta) \end{aligned} \quad (8)$$

$$\begin{aligned} & \frac{1}{r} \frac{\partial}{\partial \theta} \left(\frac{3h_o^2 r \cos\theta}{12\mu r} p_o \frac{\partial p_o}{\partial \theta} + \frac{h_o^3}{12\mu r} \frac{\partial(p_o p_{\varphi_y})}{\partial \theta} - \frac{B\Omega r}{2} (p_{\varphi_y} h_o + p_o r \cos\theta) \right) + \\ & \frac{1}{r} \frac{\partial}{\partial r} \left[r \left(\frac{3h_o^2 r \cos\theta}{12\mu} p_o \frac{\partial p_o}{\partial r} + \frac{h_o^3}{12\mu} \frac{\partial(p_o p_{\varphi_y})}{\partial r} \right) \right] = i\omega (p_{\varphi_y} h_o + p_o r \cos\theta) \end{aligned} \quad (9)$$

4. Finite Element Procedure for the Lubrication Equations

An efficient finite element procedure is implemented for the solution of the perturbed lubrication equations. The solution procedure is based on the Galerkin weighted residual method and uses high-order shape functions $\{\psi_j^e\}_{j=1,2,3,4}$, which are derived from an approximate solution to the non-linear Reynolds equation within an element (Faria, 2001). The fluid flow domain within the seal lands is divided into four-node isoparametric finite elements Ω_e with boundary given by Γ_e . The zeroth-order pressure field is interpolated over the element domain in the following form.

$$p_o^e = \sum_{i=1}^4 \psi_i^e p_{o_i}^e \quad (10)$$

where $p_{o_i}^e$ are the nodal values of pressure on the element (e). By employing the Galerkin weighted residual method and substituting Eq. (10) into Eq. (6) render the following zeroth-order finite element system of asymmetric equations

$$K_{ji}^e \cdot p_{o_i}^e = q_j^e, \quad i,j=1,2,3,4 \quad (11)$$

where

$$K_{ji}^e = \iint_{\Omega_e} \left\{ \frac{p_o h_o^3}{12\mu} \left(\frac{\partial \psi_i^e}{\partial r} \frac{\partial \psi_j^e}{\partial r} + \frac{1}{r^2} \frac{\partial \psi_i^e}{\partial \theta} \frac{\partial \psi_j^e}{\partial \theta} \right) - \frac{B\Omega h_o}{2} \psi_i^e \frac{\partial \psi_j^e}{\partial \theta} \right\} d\Omega_e \quad (12)$$

$$q_j^e = - \oint_{\Gamma_e} \psi_j^e \dot{m}_n d\Gamma_e \quad (13)$$

\dot{m}_n is the zeroth-order mass flow rate normal to the element boundary. A successive substitution procedure is implemented to solve iteratively the system of zeroth-order finite element equations (Faria, 2001).

The finite element equations for the first-order pressures are obtained in a similar way. The pressures p_z , p_{φ_x} , and p_{φ_y} are interpolated within an element domain in the following form.

$$p_z^e = \sum_{i=1}^4 \Psi_i^e p_{z_i}^e, \quad p_{\varphi_x}^e = \sum_{i=1}^4 \Psi_i^e p_{\varphi_{x_i}}^e \quad \text{and} \quad p_{\varphi_y}^e = \sum_{i=1}^4 \Psi_i^e p_{\varphi_{y_i}}^e. \quad (14)$$

Then the finite element first-order equation for axial displacements Z is expressed as

$$K_{z_{ji}}^e \cdot p_{z_i}^e = q_{z_j}^e + f_{z_j}^e, \quad i,j=1,2,3,4 \quad (15)$$

where

$$K_{z_{ji}}^e = \iint_{\Omega_e} \left[\frac{p_o^e h_o^3}{12\mu} \left(\frac{\partial \Psi_j^e}{\partial r} \frac{\partial \Psi_i^e}{\partial r} + \frac{1}{r^2} \frac{\partial \Psi_j^e}{\partial \theta} \frac{\partial \Psi_i^e}{\partial \theta} \right) + \frac{h_o^3}{12\mu} \left(\frac{\partial \Psi_j^e}{\partial r} \frac{\partial p_o^e}{\partial r} + \frac{1}{r^2} \frac{\partial \Psi_j^e}{\partial \theta} \frac{\partial p_o^e}{\partial \theta} \right) \Psi_i^e - \frac{B\Omega h_o}{2} \frac{\partial \Psi_j^e}{\partial \theta} \Psi_i^e + i\omega h_o \Psi_j^e \Psi_i^e \right] d\Omega_e \quad (16)$$

$$q_{z_j}^e = - \oint_{\Gamma_e} \Psi_j^e \dot{m}_{z_n} d\Gamma_e \quad (17)$$

$$f_{z_j}^e = \iint_{\Omega_e} \left(\frac{-3h_o^2}{12\mu} p_o^e \left(\frac{\partial \Psi_j^e}{\partial r} \frac{\partial p_o^e}{\partial r} + \frac{1}{r^2} \frac{\partial \Psi_j^e}{\partial \theta} \frac{\partial p_o^e}{\partial \theta} \right) + \frac{B\Omega p_o^e}{2} \frac{\partial \Psi_j^e}{\partial \theta} - i\omega p_o^e \Psi_j^e \right) d\Omega_e. \quad (18)$$

The first-order mass flow rate outward the element boundary is given by \dot{m}_{z_n} .

The finite element systems of equations for the first-order equations for angular displacements φ_x and φ_y are given by

$$K_{\varphi_{x_{ji}}}^e \cdot p_{\varphi_{x_i}}^e = q_{\varphi_{x_j}}^e + f_{\varphi_{x_j}}^e, \quad i,j=1,2,3,4 \quad (19)$$

$$K_{\varphi_{y_{ji}}}^e \cdot p_{\varphi_{y_i}}^e = q_{\varphi_{y_j}}^e + f_{\varphi_{y_j}}^e, \quad i,j=1,2,3,4 \quad (20)$$

where

$$K_{\varphi_{x_{ji}}}^e = K_{z_{ji}}^e \quad (21)$$

$$K_{\varphi_{y_{ji}}}^e = K_{z_{ji}}^e \quad (22)$$

$$q_{\varphi_{x_j}}^e = - \oint_{\Gamma_e} \Psi_j^e \dot{m}_{x_n} d\Gamma_e \quad (23)$$

$$q_{\varphi_{y_j}}^e = - \oint_{\Gamma_e} \Psi_j^e \dot{m}_{y_n} d\Gamma_e \quad (24)$$

$$f_{\varphi_{x_j}}^e = \iint_{\Omega_e} \left\{ \frac{3h_o^2 r \sin\theta}{12\mu} p_o^e \left(\frac{\partial \Psi_j^e}{\partial r} \frac{\partial p_o^e}{\partial r} + \frac{1}{r^2} \frac{\partial \Psi_j^e}{\partial \theta} \frac{\partial p_o^e}{\partial \theta} \right) - \frac{B\Omega r \sin\theta}{2} p_o^e \frac{\partial \Psi_j^e}{\partial \theta} + i\omega p_o^e r \sin\theta \Psi_j^e \right\} d\Omega_e \quad (25)$$

$$f_{\varphi_{y_j}}^e = \iint_{\Omega_e} \left\{ \frac{-3h_o^2 r \cos\theta}{12\mu} p_o^e \left(\frac{\partial \Psi_j^e}{\partial r} \frac{\partial p_o^e}{\partial r} + \frac{1}{r^2} \frac{\partial \Psi_j^e}{\partial \theta} \frac{\partial p_o^e}{\partial \theta} \right) + \frac{B\Omega r \cos\theta}{2} p_o^e \frac{\partial \Psi_j^e}{\partial \theta} - i\omega p_o^e r \cos\theta \Psi_j^e \right\} d\Omega_e \quad (26)$$

where \dot{m}_{x_n} and \dot{m}_{y_n} are the first-order mass flow rates outward Γ_e .

5. Steady-State and Dynamic Performance Characteristics

The finite element equations (11), (15), (19) e (20) are assembled for the whole seal domain. The zeroth- and first-order pressure fields are computed by solving the global finite element equations (Faria, 2001). Seal opening force (F_z) and restoring moments ($M_{\varphi_x}, M_{\varphi_y}$) are given by the following expression.

$$\begin{Bmatrix} F_z \\ M_{\varphi_x} \\ M_{\varphi_y} \end{Bmatrix} = \iint_{\Omega} \begin{Bmatrix} (p_o - p_{ref}) \\ -(p_o - p_{ref})r \sin\theta \\ (p_o - p_{ref})r \cos\theta \end{Bmatrix} r d\theta dr \quad (27)$$

where p_{ref} represents the reference pressure defined as the lowest pressure of the seal inner and outer pressures. The dynamic force and moment coefficients are given by

$$K_{\sigma\beta} + i\omega C_{\sigma\beta} = -\iint_{\Omega} h_{\sigma} p_{\beta} r d\theta dr \quad , \quad \sigma, \beta = Z, \varphi_x, \varphi_y \quad (28)$$

where $h_z = 1$, $h_{\varphi_x} = -r \sin\theta$, and $h_{\varphi_y} = r \cos\theta$. Equation (28) is rewritten in matrix form as

$$\begin{bmatrix} K_{zz} & K_{z\varphi_x} & K_{z\varphi_y} \\ K_{\varphi_x z} & K_{\varphi_x \varphi_x} & K_{\varphi_x \varphi_y} \\ K_{\varphi_y z} & K_{\varphi_y \varphi_x} & K_{\varphi_y \varphi_y} \end{bmatrix} + i\omega \begin{bmatrix} C_{zz} & C_{z\varphi_x} & C_{z\varphi_y} \\ C_{\varphi_x z} & C_{\varphi_x \varphi_x} & C_{\varphi_x \varphi_y} \\ C_{\varphi_y z} & C_{\varphi_y \varphi_x} & C_{\varphi_y \varphi_y} \end{bmatrix} = \iint_{\Omega} \begin{Bmatrix} -1 \\ r \sin\theta \\ -r \cos\theta \end{Bmatrix} \begin{Bmatrix} p_z \\ p_{\varphi_x} \\ p_{\varphi_y} \end{Bmatrix} r d\theta dr \quad (29)$$

6. Numerical Results

Firstly, an analysis of a SGGFS case is carried out to validate the finite element procedure developed in this work. Secondly, some dynamic performance characteristics are evaluated for an inward pumping spiral groove gas seal employed in nitrogen pumps in order to study the influence of the angular misalignment and the face coning on the behavior of grooved gas face seals.

6.1. Validation

An example of aligned high-speed SGGFS is selected to validate the FEM procedure implemented in this work. The seal opening force and the static axial stiffness predicted by the FEM procedure are compared with computed results presented by Gabriel (1994). The seal parameters are presented in Tab. (1). The speed number (Λ), which is shown in Tab. (1), is computed by $\Lambda = \frac{6\mu\Omega}{p_{ref}} \left(\frac{r_o}{c} \right)^2$.

Table 1. SGGFS parameters for validation.

$r_i = 0.05842$ m	(stationary grooves)	c varies
$r_{gi} = 0.069$ m	$\Omega = 28,600$ rpm	$c_g = 5$ μ m
$r_o = 0.07778$ m	$\rho = 1.12$ kg/m ³	$\mu = 18 \times 10^{-6}$ Pa.s
$\beta = 165^\circ$	Lubricant: Air	$p_{in} = 0.1013$ MPa
$N_g = 10$ grooves		$p_{out} = 4.5852$ MPa
$\alpha_g = 0.5$		Λ varies from 749 to 4688

Figures (4) and (5) depict the comparative results of seal opening force and axial static stiffness versus ridge clearance computed for the seal parameters given in Tab. (1). The seal domain is modeled with 1100 finite elements. There is a good agreement between the FEM predictions and the results presented by Gabriel (1994).

6.2. Performance Characteristics of SGGFSs

The influence of the static misalignment and the face coning on the performance characteristics of spirally grooved gas face seals is analyzed at moderate and high speed numbers (Λ). The seal baseline geometry for this analysis is given in Tab. (2), and represents a high speed inward pumping SGGFS employed in nitrogen pumps.

Table 2. Geometric and operating parameters for a SGGFS.

<i>Stationary grooves</i>		
$r_i = 0.07112$ m	$\beta = 160^\circ$	$p_{in} = 0.101$ MPa
$r_{gi} = 0.076454$ m	$\alpha_g = 0.5$	$p_{out} = 0.505$ MPa
$r_o = 0.0889$ m	$N_g = 12$ grooves	$\Lambda = 300$ or 1253
$c = c_g = 2.54$ μm	$\mu = 10.963 \times 10^{-6}$ Pa.s	$(\Omega = 3600$ or 15000 rpm)
<i>Mesh: 1320 elements</i>		
<i>(132 circumferential x 10 radial elements)</i>		

Firstly, some performance characteristics of a perfectly symmetric, aligned SGGFS operating at high speeds are evaluated in relation to positive ($\gamma > 0$) and negative ($\gamma < 0$) coning angles. The seal clearance at the outer radius increases for ($\gamma > 0$) and decreases for ($\gamma < 0$) (see Figure (2)). Table (3) shows the normalization of the seal opening force (\bar{F}_z), leakage flow rate (\bar{Q}), stiffness coefficients (\bar{K}_{ij}), and damping coefficients (\bar{C}_{ij}) employed in this analysis.

The seal performance characteristics are determined at moderate ($\Lambda=300$) and high speed numbers ($\Lambda=1253$), and are depicted in relation to the dimensionless coning parameter coning parameter ($\bar{\gamma}$), which is defined as

$$\bar{\gamma} = \gamma \cdot (\pi \cdot r_o / 180 \cdot c) \quad \text{for positive } \gamma \quad (30.a)$$

$$\bar{\gamma} = 5\gamma \cdot (\pi \cdot r_o / 180 \cdot c) \quad \text{for negative } \gamma \quad (30.b)$$

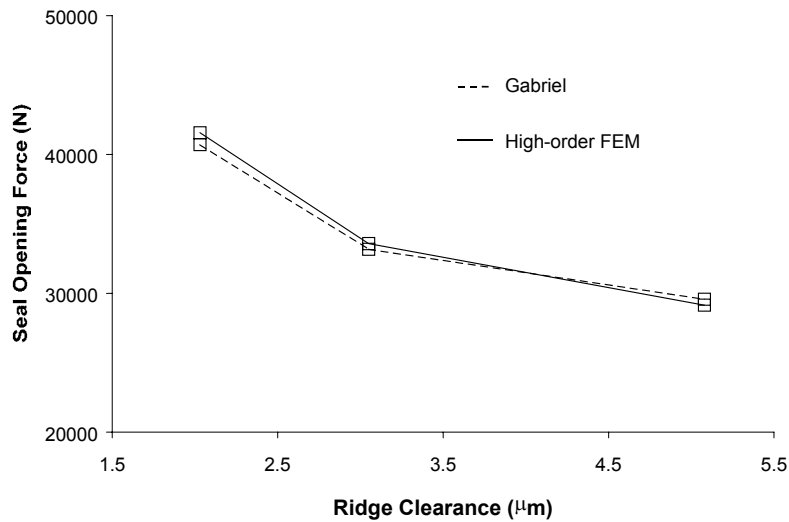


Figure 4. Comparative results for seal opening force in a SGGFS.

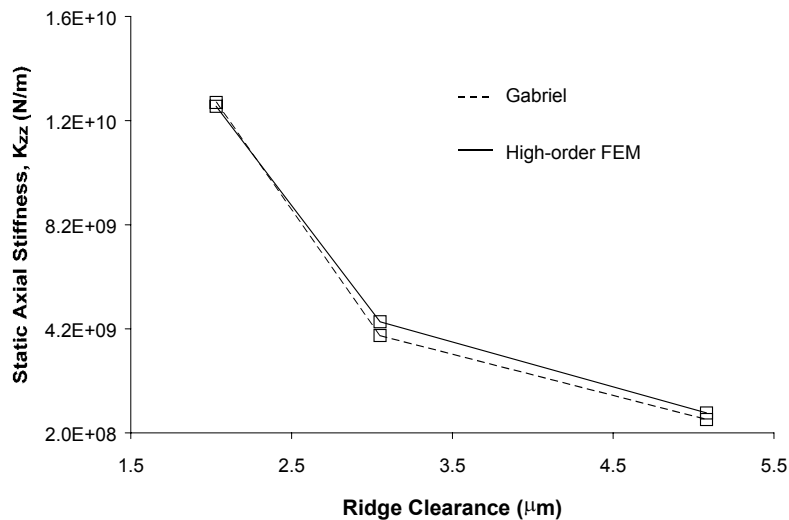


Figure 5. Comparative results for axial static stiffness in a SGGFS.

Table 3. Normalization parameters for seal performance characteristics.

$\bar{F}_z = F_z / F^*$	$F^* = p_{av}\pi(r_o^2 - r_i^2)$	$p_{av} = (p_o + p_i)/2$
$\bar{Q} = Q/Q^*$	$Q^* = \frac{\pi p_{av}(c + c_g)^3 p^*}{6\mu \ln(r_o/r_i)}$	$\rho_{av} = \frac{p_o + p_i}{2R_g T}$
	where $p^* = (p_i - p_o)$	
Axial stiffness :	$\bar{K}_{zz} = K_{zz}/K_{zz}^*$	$K_{zz}^* = F^*/c$
Angular stiffness:	$\bar{K}_{ij} = K_{ij}/K_{xx}^* ; i,j=\varphi_x,\varphi_y$	$K_{xx}^* = \frac{F^* r_o^2}{c}$
Cross-Coupled Stiffness:	$\bar{K}_{zi} = K_{zi}/K_{xz}^* ; i=\varphi_x,\varphi_y$ $\bar{K}_{iz} = K_{iz}/K_{xz}^*$	$K_{xz}^* = F^* r_o/c$
Axial damping :	$\bar{C}_{zz} = C_{zz}/C_{zz}^*$	$C_{zz}^* = K_{zz}^*/\Omega$
Angular damping :	$\bar{C}_{ij} = C_{ij}/C_{xx}^* ; i,j=\varphi_x,\varphi_y$	$C_{xx}^* = C_{zz}^* r_o^2$
Cross-Coupled Damping:	$\bar{C}_{zi} = C_{zi}/C_{xz}^* ; i=\varphi_x,\varphi_y$ $\bar{C}_{iz} = C_{iz}/C_{xz}^*$	$C_{xz}^* = F^* r_o/c \Omega$

with different scales for negative and positive coning angles for graphical representation purpose. A negative γ implies the seal outer clearance decreases, while positive γ increases the outer clearance. Rubbing contact between the seal mating faces occurs at approximately $\gamma = -0.008^\circ$. In this study, the minimum value of coning parameter corresponds to an almost zero outer clearance (about 90% of reduction), while the maximum coning parameter corresponds to an outer clearance four times larger than the seal inner clearance.

Figure (6) depicts the variation of \bar{Q} and \bar{F}_z with the coning parameter at moderate (dashed line) and high speed numbers (solid line). As the outer clearance decreases (γ decreases), the flow resistance increases resulting in higher opening force and lower inward flow. \bar{Q} and \bar{F}_z increase as the speed number (Λ) increases due to the increase in the hydrodynamic pressure over the seal domain. Figure (7) shows the static axial and angular stiffness and damping coefficients versus coning parameter at moderate (dashed line) and high speed numbers (solid line).

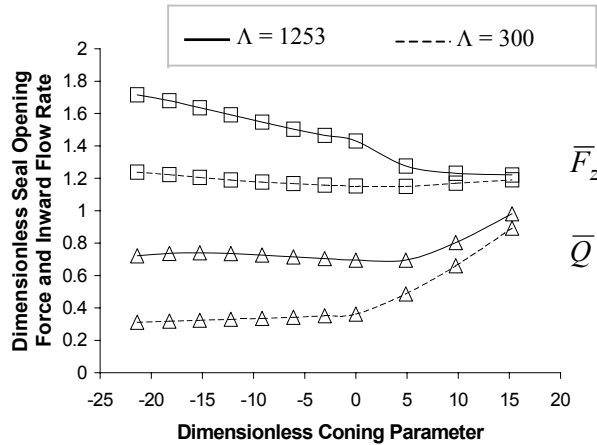


Figure 6. Dimensionless opening force and inward flow rate versus coning parameter.

For zero misalignment, the force coefficients associated with the coupling between the axial and angular motions are null ($K_{z\varphi_x}, K_{z\varphi_y}, C_{z\varphi_x}, C_{z\varphi_y} = 0$), the angular direct coefficients are equal ($K_{\varphi_x\varphi_x} = K_{\varphi_y\varphi_y}, C_{\varphi_x\varphi_x} = C_{\varphi_y\varphi_y}$) and the angular cross-coupled coefficients are skew-symmetric ($K_{\varphi_x\varphi_y} = -K_{\varphi_y\varphi_x}, C_{\varphi_x\varphi_y} = -C_{\varphi_y\varphi_x}$). These coefficients are evaluated at a very low axial excitation frequency ($\omega \cong 0$). Stiffness and damping coefficients increase as the outer clearance decreases ($\bar{\gamma} < 0$) because of the increasing flow resistance. For small outer clearances ($\bar{\gamma} < -12$), the direct axial damping (\bar{C}_{zz}) increases significantly as the coning angle decreases at high speed number ($\Lambda = 1253$). High speed results in high flow resistance causing this abrupt increase in the direct axial damping. The angular direct damping coefficient ($\bar{C}_{\varphi_x\varphi_x}$) becomes negative for negative coning angles at high speed ($\Lambda = 1253$).

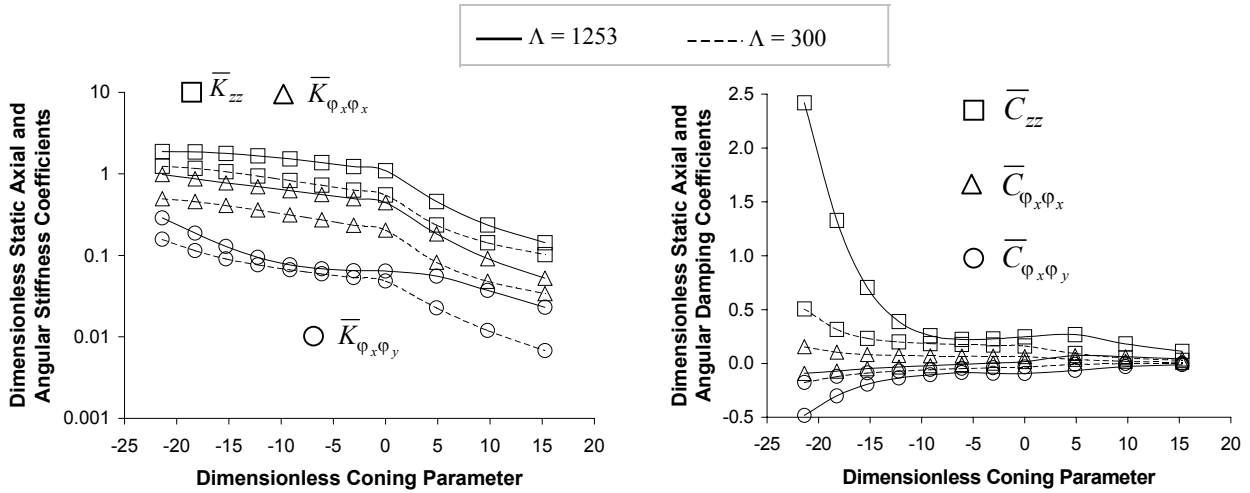


Figure 7. Dimensionless static stiffness and damping coefficients versus coning parameter in a SGGFS.

Now, the seal performance characteristics are evaluated with respect to the static misalignment about the axis X . In this study, the fixed seal face (stationary face) is slightly misaligned and the flexibly mounted face is perfectly aligned. Coning effects are not taken into account in the computations. The misalignment angle is given in degrees. The minimum and maximum values of seal outer clearances are about $0.9 \mu\text{m}$ and $4.1 \mu\text{m}$ (for $\varphi_x = 0.001^\circ$), respectively. Figure (8) shows the dimensionless seal opening force (\bar{F}_z) and inward flow rate (\bar{Q}) versus misalignment about the axis X (φ_x) at moderate (dashed line) and high speed numbers (solid line). \bar{Q} and \bar{F}_z increase with increasing φ_x . The misalignment generates regions of converging and diverging clearances in the circumferential direction. The hydrodynamic pressure increases in the region of converging clearances.

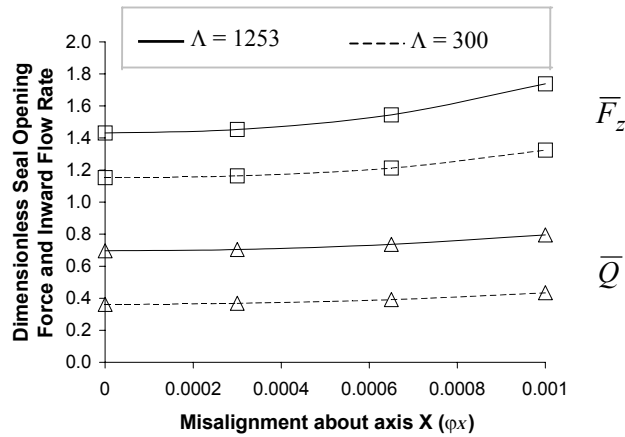


Figure 8. Dimensionless opening force and flow rate versus misalignment angle in a SGGFS.

The direct stiffness coefficients increase as φ_x increases for moderate and high speed numbers, while direct damping coefficients decrease as misalignment angle increases (Faria, 2002). For brevity, the curves of direct force coefficients versus misalignment are not shown. Figure (9) shows the static cross-coupled stiffness and damping coefficients at high speed ($\Lambda=1253$) number. As expected, the cross-coupled stiffness coefficients associated with the coupling between the axial and tilt motions ($\bar{K}_{z\varphi_x}, \bar{K}_{\varphi_x z}$) vary significantly with increasing misalignment angle about axis X . The cross-coupled coefficients $\bar{C}_{z\varphi_x}$ and $\bar{C}_{\varphi_x z}$ increase significantly as misalignment angle about axis X increases. Negative direct damping coefficients indicate that large misalignment angles can induce unstable axial and angular motions at high speed numbers.

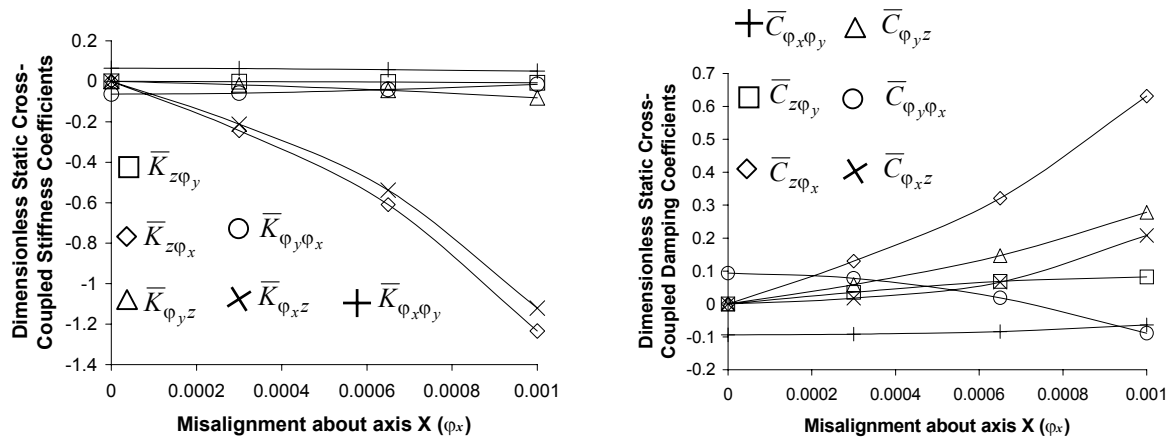


Figure 9. Dimensionless cross-coupled static force coefficients versus misalignment angle in a SGGFS ($\Lambda = 1253$).

7. Conclusions

The finite element procedure implemented in this work is able to analyze spiral groove gas face seals (SGGFSs) operating at high speeds accounting for the seal face static misalignment and coning. This procedure can efficiently predict some steady-state performance characteristics, such as the seal opening force and leakage flow rate, and some dynamic performance characteristics, such as the stiffness and damping force coefficients. The numerical results presented in this work show the influence of the angular misalignment between seal faces and the face coning on the behavior of SGGFSs under stringent operating conditions. Angular misalignment between the seal faces and face coning are common features in gas face seals operating at high speeds. The analysis shows that negative coning and large misalignment angles can induce negative direct angular damping coefficients at high Λ making the seal more susceptible to angular motions. Negative or divergent face coning ($\gamma < 0$) also results in increased seal opening force and stiffness coefficients offering increasing resistance to rubbing contact between the seal mating faces.

8. References

- Burgmann Dichtungswerke GmbH & Co., 1997, "Gas Lubricated Mechanical Face Seals", First Edition, Wolfratshausen, Germany, 76 p.
- Faria, M. T. C., 2001, "An Efficient Finite Element Procedure for Analysis of High-Speed Spiral Groove Gas Face Seals", ASME Journal of Tribology, Vol. 123, No. 1, pp. 205-210.
- Faria, M.T.C., 2002, "Misalignment Effects on the Behavior of Spiral Groove Gas Face Seals", Proceedings of the 9th Brazilian Congress of Thermal Engineering and Sciences, Caxambu, MG, Brazil, pp.1-11.
- Gabriel, R.P., 1994, "Fundamentals of Spiral Groove Noncontacting Face Seals", STLE Lubrication Engineering, March, pp.215-224.
- Jang, G.H., and Kim, Y.J., 1999, "Calculation of Dynamic Coefficients in a Hydrodynamic Bearing Considering Five Degrees of Freedom for a General Rotor-Bearing System", ASME Journal of Tribology, Vol.121, No. 3, pp. 499-505.
- Lund, J.W., 1987, "Review of the Concept of Dynamic Force Coefficients for Fluid Film Journal Bearings", ASME Journal of Tribology, Vol.109, No. 1, pp. 37-40.
- Metcalf, R., 1981, "Dynamic Tracking of Angular Misalignment in Liquid-Lubricated End-Face Seals", ASLE Transactions, Vol. 24, No. 4, pp. 509-516.
- Muijderman, E.A., 1966, "Spiral Groove Bearings", Philips Technical Library, Springer-Verlag, New York, 212 p.
- Pan, C. H. T. and Sternlicht, B., 1967, "Thermal Distortion of Spiral-Grooved Gas-Lubricated Thrust Bearing Due to Self-Heating", ASME Journal of Lubrication Technology, Vol. 89, pp. 197-202.
- Sharoni, A. and Etsion, I., 1981, "Performance of End-Seals with Diametral Tilt and Coning – Hydrodynamic Effects", ASLE Transactions, Vol. 24, No. 1, pp. 61-70.
- Tournerie, B., Huitric, J., Bonneau, D. and Frene, J., 1994, "Optimisation and Performance Prediction of Grooved Face Seals for Gases and Liquids", Proceedings of the 14th International Conference on Fluid Sealing, Firenze, Italy, pp. 351-365.
- Wileman, J. and Green, I., 1991, "The Rotordynamic Coefficients of Mechanical Seals Having Two Flexibly Mounted Rotors", ASME Journal of Tribology, Vol. 113, pp. 795-804.

9. Copyright Notice

The author is the only responsible for the printed material included in his paper.